JOURNAL OF MORPHOLOGY 273:441–452 (2012)

Regional Variation in Morphology of Vertebral Centra and Intervertebral Joints in Striped Bass, *Morone saxatilis*

B.N. Nowroozi,[1]* C.J. Harper,[1] B. De Kegel,[2] D. Adriaens,[2] and E.L. Brainerd[1]

[1]*Department of Ecology and Evolutionary Biology, Brown University, Providence, Rhode Island 02912*
[2]*Evolutionary Morphology of Vertebrates, Ghent University, Gent 9000, Belgium*

ABSTRACT The vertebral column of fishes has traditionally been divided into just two distinct regions, abdominal and caudal. Recently, however, developmental, morphological, and mechanical investigations have brought this traditional regionalization scheme into question. Alternative regionalization schema advocate the division of the abdominal vertebrae into cervical, abdominal, and in some cases, transitional regions. Here, we investigate regional variation at the level of the vertebrae and intervertebral joint (IVJ) tissues in the striped bass, *Morone saxatilis*. We use gross dissection, histology, and polarized light imaging to quantify vertebral height, width, length, IVJ length, IVJ tissue volume and cross-sectional area, and vertical septum fiber populations, and angles of insertion. Our results reveal regional differences between the first four (most rostral) abdominal vertebrae and IVJs and the next six abdominal vertebrae and IVJs, supporting the recognition of a distinct cervical region. We found significant variation in vertebral length, width, and height from cranial to caudal. In addition, we see a significant decline in the volume of notochordal cells and the cross-sectional area of the fibrous sheath from cranial to caudal. Further, polarized light imaging revealed four distinct fiber populations within the vertical septum in the cervical and abdominal regions in contrast with just one fiber population found in the caudal region. Measurement of the insertion angles of these fiber populations revealed significant differences between the cervical and abdominal regions. Differences in vertebral, IVJ, and vertical septum morphology all predict greater range of motion and decreased stiffness in the caudal region of the fish compared with the cervical and abdominal regions. J. Morphol. 273:441–452, 2012.

KEY WORDS: vertebral column; intervertebral joints; *Morone saxatilis*; vertebrae; regionalization

INTRODUCTION

Regionalization of the vertebral column has been identified across a variety of vertebrate taxa (Heilman, 1927; Romer, 1956; Wake and Lawson, 1973; Wake, 1980). Typically, this regionalization is defined based on variation in morphology and mechanics along the length of the spine. For example, in humans, we see regionalization of the vertebral column based on the size and shape of vertebral centra as well as the presence or absence of ribs. Mechanically, the lumbar region of the human vertebral column has a smaller range of motion, and greater mechanical stiffness compared with the more flexible cervical region (Panjabi et al., 1976; White and Panjabi, 1978; Panjabi et al., 1994; Panjabi et al., 2001; Kulig et al., 2007; McDonald et al., 2010). Similarly, the regionalization of the fish axial skeleton has been defined based on vertebral morphology.

The vertebral column of actinopterygian fishes has traditionally been divided into two regions, commonly termed abdominal and caudal (e.g., Bond, 1996; Grande and Bemis, 1998; Kacem et al., 1998; Ward and Brainerd, 2007), but also called trunk and tail (e.g., Gadow and Abbott, 1895), trunk and caudal (e.g., Kardong, 1998; Liem et al., 2001), and precaudal and caudal (e.g., Rockwell et al., 1938; Bird and Mabee, 2003). Although the number of vertebrae in these two regions can be highly variable, even within a species (Ward and Brainerd, 2007), the regions are defined primarily by longitudinal position relative to the anus and the presence or absence of ribs and hemal spines (Rockwell et al., 1938; Helfman et al., 1997). The abdominal vertebrae are located anterior to the anus and they generally bear ribs, with the exception of the most rostral vertebrae in some species. The caudal vertebrae are defined as the hemal spine-bearing vertebrae located posterior to the anus.

Recently, however, these traditional abdominal and caudal divisions have been called into question.

Contract grant sponsor: US National Science Foundation; Contract grant number: 0629372; Contract grant sponsors: Bushnell Graduate Education and Research Fund, Sigma Xi Grant-in-Aid of Research.

*Correspondence to: Bryan N. Nowroozi, 80 Waterman St., Box G-W, Providence, RI 02912. E-mail: bryan_nowroozi@brown.edu

Received 22 July 2011; Revised 10 September 2011;
Accepted 1 October 2011

Published online 23 November 2011 in
Wiley Online Library (wileyonlinelibrary.com)
DOI: 10.1002/jmor.11034

Studies of zebrafish development have suggested that the pattern of ossification, as well as Hox gene expression, result in distinct cervical and transitional regions of the vertebral column in addition to the abdominal and caudal regions (Morin-Kensicki et al., 2002, Bird and Mabee, 2003). Of particular importance, the expression of *hoxc6* has been shown to align with the border between the cervical (nonrib bearing) and abdominal (rib-bearing) vertebrae in zebrafish (Morin-Kensicki et al., 2002). The same *Hoxc6* expression correlates with the border between cervical to thoracic vertebrae in both the chick and mouse, suggesting similarities in this regionalization across taxa (Burke et al., 1995). In addition, evidence suggests the anterior expression border of *hoxd12* may correspond to a transitional region intermediate in morphology between the abdominal and caudal regions (Bird and Mabee, 2003). Thus, Hox gene expression in zebrafish suggests regionalization from anterior to posterior of cervical, abdominal, transitional, and caudal.

In addition, the results of mechanical tests on various species suggest different species-specific regionalization schema. In the blue marlin, *Makaira nigricans*, mechanical tests show an increase in angular stiffness in the caudal region, suggesting a mechanical division between the traditional abdominal and caudal joints (Hebrank et al., 1990; Long, 1992). However, a comparative study on skipjack tuna (*Katsuwonus pelamis*) and Norfolk spot (*Leisostomus xanthurus*) found mechanical regionalization in angular stiffness of intervertebral joints (IVJs) along the vertebral column divided into abdominal, caudal peduncle, and caudal fin associated joints in the skipjack tuna, whereas uniform mechanics along the length of the vertebral column were reported in the Norfolk spot (Hebrank, 1982).

Most previous morphological analyses of regionalization in fishes have been based on gross morphology of vertebrae, and very little is known about the regional variation in soft tissue anatomy of the IVJs. The IVJ tissues likely play an important role in the mechanical properties of each joint along the length of the vertebral column, and should be included in a regionalization analysis. In amphicoelous fish vertebrae, the IVJ structures are housed within two adjacent vertebrae (Fig. 1). IVJ soft tissue structures can be divided into two classes: the tissues that encapsulate the notochordal remnants (encapulating complex), and the notochordal remnants themselves [the notochordal cell mass (NCM), the notochordal epithelium (NE), and the notochordal strand, (Nst)].

The tissues that form the encapsulating complex (i.e., the joint capsule) consist of the fibrous sheath, the elastica externa, and the external intervertebral ligament (Schmitz, 1995; Nordvik et al., 2005). Lying between the two vertebrae and extending just deep to the bone of the vertebra is

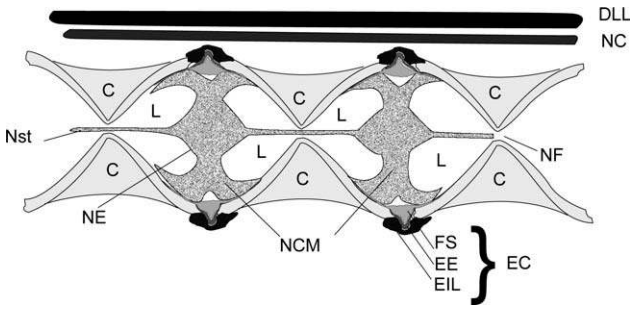

Fig. 1. Sagittal section schematic of three amphicoelous vertebral centra and two intervertebral joints (IVJs). Adapted from Symmons, 1979. Abbreviations: C, centrum; DLL, dorsal longitudinal ligament; EC, encapsulating complex; EE, elastica externa; EIL, external intervertebral ligament; FS, fibrous sheath; L, lacunae; NC, nerve cord; NCM, notochordal cell mass; NE, notochordal epithelium; NF, notochordal foramen; Nst, notochordal strand.

the fibrous sheath (Fig. 1). The fibrous sheath is a helically wound structure in both the shortnose sturgeon (*Acipenser brevirostratus*) and African lungfish (*Protopterus annectens*), and can be acellular, as seen in the sturgeon, or contain fibroblasts, as seen in the lungfish (Schmitz, 1998). Because of the putative homology of the fibrous sheath with that of other craniates, it has been suggested that this tissue is composed of Type II collagen and associated proteoglycans in fishes (Linsenmayer et al., 1973; Kimura and Kamimura, 1982; Eikenberry et al., 1984; Schmitz, 1998; Grotmol et al., 2006). Between the rims of the two vertebrae, two additional encapsulating tissues can be found. The first is the elastica externa, an elastic layer positioned superficially to the fibrous sheath. Superficial to that elastic layer is a layer composed of sclerotomally derived collagen called the external intervertebral ligament (Fig. 1). Each of the three tissues within the encapsulating complex is thought to resist tensile loading during the lateral bending of locomotion (Symmons, 1979, Schmitz, 1995, 1998).

Within the IVJ capsule, the cellular remnants of the notochordal tissue form the notochordal cell mass, notochordal strand, and notochordal epithelium (Fig. 1). The notochordal cell mass consists of notochordal cells of varying degrees of vacuolization with each vacuole surrounded by networks of intermediate filaments. These dense filamentous networks of adjacent cells are connected to one another by desmosomes that promote cell-to-cell adhesion, allowing the vacuoles to resist compressive loads as the filaments distribute this load (Schmitz, 1995; Junqueira and Carneiro, 2005). The notochordal strand, thought to be present only in basal ray-finned fishes, runs longitudinally along the length of the vertebral column passing through the center of each amphicoel via a notochordal foramen (Fig. 1). Previous studies suggest that this axial strand is under a tensile load that

TABLE 1. Summary of individual Morone saxatilis

	Total length (m)	Body mass (kg)
Gross morphology		
Individual 01	0.36	0.52
Individual 02	0.95	11.11
Individual 03	0.66	3.35
Individual 04	0.32	0.43
Individual 05	0.34	0.45
Histology		
Individual 06	0.26	0.33
Individual 07	0.28	0.39
Individual 08	0.28	0.36
Polarized light		
Individual 09	0.33	0.73
Individual 10	0.35	0.41
Individual 11	0.28	0.42

might play a role in elastic resilience during locomotion (Symmons, 1979). In the persistant notochord of sturgeon and lungfishes, this strand is composed of the intermediate filaments of collapsed vacuolated notochordal cells (Schmitz, 1998). The last of the remnants of the notochordal tissues is a lining composed of a thin layer of notochordal cells called the notochordal epithelium. This tissue separates the two extracellular lacunae from the notochordal cell mass. The lacunae are fluid filled spaces that occupy a substantial portion of the IVJ cavity and are thought to resist compressive loads related to locomotion (Schmitz, 1995), and possibly supply nutrients to the notochordal cell mass (Symmons, 1979) (Fig. 1).

Finally, there are two tissues that lie external to the IVJ capsule that we have included in our investigation: the dorsal longitudinal ligament and the vertical septum. The dorsal longitudinal ligament passes through the neural arch and lies dorsal to the nerve chord (Fig. 1). The vertical septum is a sheet of connective tissue that spans the area between adjacent neural and hemal spines. Both of these tissues have been implicated in resisting lateral bending and contributing to elastic energy storage during locomotion (Symmons, 1979; Videler, 1993). In particular, the vertical septum is thought to store energy elastically not only in the fibers of the connective tissue but also by transferring load to the associated neural and hemal spines (Videler, 1993). Given these hypotheses, any variation in these tissues will impact the mechanics of IVJ function during locomotion.

The primary goals of the present study are: (1) to describe and quantify regional variation in the morphology of the vertebral centra and IVJ tissues along the length of the vertebral column of an actinopterygian fish; (2) to determine whether this variation supports any of the proposed regionalization schema in fishes; and (3) to hypothesize how regional variation might affect the mechanical performance of the IVJs. We use gross dissection, serial sectioning of IVJs, and polarized light imaging of the vertical septum to investigate this variation. We focused our investigation on the striped bass, *Morone saxatilis* (Walbaum), a perciform fish with relatively small number of vertebrae (24) compared with other fishes of similar size. The low vertebral number results in larger vertebrae and IVJs, which should facilitate our morphological measurements as well as future mechanical and *in vivo* studies. In addition, the striped bass swims with a nonspecialized, subcarangiform swimming style that we hope will be a general case study from which we can later compare the more specialized swimming species.

MATERIALS AND METHODS

Specimens

We studied a total of 11 striped bass, *M. saxatilis*, by gross dissection, histology, and polarized light imaging. Individuals varied in size from 0.17 m to 0.95 m in total length (TL) and 0.20 kg to 11.1 kg in body mass (Table 1). The two largest specimens, 0.95 m in length and 0.66 m in length, were obtained from local fish markets and freshly dissected for morphological measurements on the same day. The remaining nine individuals were obtained live from the Susquehanna Aquaculture, fish hatchery (York Haven, PA) and housed in a 300 gallon circular aquarium at 19–22°C. Individuals of relatively similar TL and weight were chosen for both the histology and polarized light imaging of the vertical septum. Conversely, individuals of diverse lengths and weights were used for gross morphological measurements (Table 1).

Morphological Measurements

Five individuals of *M. saxatilis* (Table 1) were studied by gross dissection and measurements were made using Mitotoyo digital calipers. Measurement precision was determined to be ±0.02 mm based on the standard deviation of 50 repeated measurements of the length of a single vertebra. To preserve the natural hydration of the IVJs, all individuals were freshly dissected (i.e., specimens were never frozen and thawed).

The axial musculature was removed from the axial skeleton and measurements were made of the length of the IVJs. This length was taken as the distance between the rims of adjacent vertebrae at the level of the lateral ridge (Fig. 2). We repeated each measurement three times and report the mean for each IVJ. Once this measurement had been made for each IVJ along the length of the vertebral column, the vertebrae were disarticulated from one another and the remaining tissue removed to facilitate centrum measurements.

For each individual centrum, we measured vertebral length, vertebral width, and vertebral height. Vertebral length was measured along the lateral ridge of each centrum. Vertebral height and width were measured from the anterior amphicoel for each vertebra (Fig. 2). For the urostyle of each individual, the length measurement was taken as the length of the rostral half amphicoel. We repeated each measurement three times and report the mean for each centrum. In addition, aspect ratio (vertebral centrum length/vertebral centrum width, see Ward and Brainerd, 2007) was calculated as a proxy for vertebral shape.

Histology

Three individuals of *M. saxatilis* were euthanized and immediately dissected to prepare for sectioning. For each individual, three vertebra-joint-vertebra specimens, called motion segments, were dissected: the most rostral motion segment included the third and fourth vertebrae, the abdominal motion

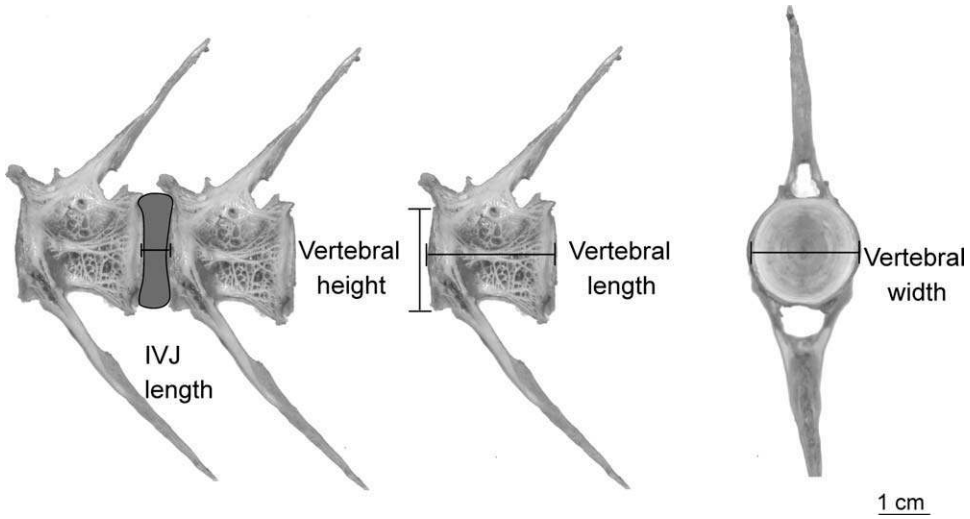

Fig. 2. Measurements of IVJ length, vertebral length, vertebral height, and vertebral width.

segment included the ninth and tenth vertebrae, and the caudal motion segment included the 20th and 21st vertebrae (vertebrae numbered from rostal to caudal in a single series).

All motion segments were then fixed in Bouin's fixative (Humason, 1979) for 3 weeks and then infiltrated and embedded into paraffin wax before sectioning. Histological sections were made in the sagittal plane using a Microm HM 360 rotational microtome (Microm International, Walldorf, Germany) at a slice thickness of 10 μm. Sections were stained using Masson's Trichrome stain (Witten and Hall, 2003) and Verhoeff's elastin stain (Gurr, 1962), and imaged under a Nikon Eclipse e600 light microscope equipped with a Nikon DXM 12000C digital camera (Nikon Instruments, Melville, NY).

For each specimen, micrographs were taken of every third section generating a stack of images with a 30 μm distance between images. This stack of images was then standardized in size and resolution and analyzed in Amira 4.0 3D visualization software (Mercury Computer Systems, Berlin, Germany). In each imaged section, the tissues were digitally dissected (i.e., segmented) by manually assigning individual pixels to specific tissue types. The segmented areas of each tissue in each section throughout the entire stack of images were then used to calculate a volume measurement for that specific tissue in each specimen. Six tissues were segmented: the notochordal cell mass, the fibrous sheath, the elastica externa, the external intervertebral ligament, and the dorsal longitudinal ligament. Three motion segments from each of three individual fish were segmented (9 tissue blocks, 1,350 total sections, and 8,100 segmented tissue areas).

For the extracellular lacunae and the notochordal cell mass, we report both the absolute volumes and the percent of the total joint cavity volume occupied by each tissue. Given the complex 3D structure of the notochordal cell mass and the fluid filled lacunae, the volume measurement provides a more accurate assessment of the tissue than a 1D length or width measurement.

For the remaining four tissues, we calculated cross-sectional area as a proxy for tissue thickness by dividing the volume of each tissue by the IVJ length. Calculations were based on volume data to reduce possible local artifacts resulting from preservation, embedding, and sectioning. Thus, we assume here that the variation in overall shrinkage of the tissues in different specimens is similar because the specimens were fixed and embedded in the same solutions for similar lengths of time. Given the vulnerability to local (within section) preservation and sectioning artifact, we feel that the cross-sectional area derived from a volume measurement that accounts for the tissue throughout the entire specimen is more accurate than a tissue thickness measurement that may be averaged over just a few regions of a few sections.

Polarized Light Imaging

Three individuals of *M. saxatilis* were euthanized and immediately dissected and prepared for imaging the vertical septum under polarized light. For each individual, motion segments taken from the same three axial positions used in the histology data set were disarticulated from the rest of the axial skeleton. The musculature and ribs were removed and each specimen was dehydrated in a graded series of acetone solutions (50%, 70%, 90%, 100%, and 100%). The specimens were then cleared in methyl salicylate and imaged under polarized light (Presnell and Schreibman, 1997; Hamilton et al., 2004; Harper et al., 2008) with a Nikon SMZ 800 stereo microscope equipped with a Nikon DXM 12000C digital camera (Nikon Instruments, Melville, NY).

Images of polarized light micrographs were analyzed using ImageJ software (National Institutes of Health, Bethesda, MD). Fibers that were oriented in similar trajectories were grouped together as a fiber population. In addition, we measured the angle of fiber insertion onto neural and hemal spines. For the majority of fiber populations, the acute angle between the fiber and the posterior spine was measured. There was one fiber population with a trajectory that ran from the vertebral centrum up to the anterior spine. Thus, the acute angle between the fiber and its insertion on the anterior spine was measured. For each population, we took 20 random fiber angle measurements and calculated the mean angle of insertion. We then calculated the mean fiber angle relative to the horizontal body axis by adding the angle between the neural or hemal spine and the horizontal body axis to the angle between the fiber population and the spine. Finally, we compared the number of fiber populations, and the normalized angles of each population, between different longitudinal regions of the three individuals.

Statistical Analysis

We analyzed data using a nested ANOVA analysis with axial position nested within individual for all three quantitative data sets: gross morphological measurements, tissue volumes from

histology, and vertical septum fiber angles. The various measurements were incorporated as the response variables. For the histological and polarized light data, differences between each pair of regions were tested post hoc using Tukey HSD multiple comparisons based on least-squared means. All statistical analyses were performed using JMP software (version 8.0.1, SAS Institute, Cary, NC).

RESULTS

Gross Morphology

The five specimens of *M. saxatilis* analyzed here for gross morphology all had 24 vertebral centra from cranial to caudal including the urostyle: 12 abdominal vertebrae, 11 caudal vertebrae, and the urostyle. Striped bass do show some intraspecific variation in vertebral number: three of the 20 specimens examined for this and related functional studies had 25 vertebrae, with the extra centrum added to the caudal series. A pair of anterior processes and a pair of posterior processes protrude from the dorsal aspects of each centrum, but the processes of adjacent vertebrae are not closely apposed. Adjacent anterior and posterior processes lie ~1–2 mm from one another *in vivo* and are bound together at the base of each process by the external intervertebral ligament. Neural spines and arches project from the dorsal aspect of each vertebral centrum.

The first 4 vertebral centra differ qualitatively from the remaining abdominal vertebrae (Fig. 3A,B). The dorsal anterior processes overlap to a greater degree with the dorsal posterior processes of the adjacent centrum. For example, the dorsal anterior processes of centrum 2 overlaps substantially with the proximal portion of the dorsal posterior processes of the first centrum near the base of the neural spine (Fig. 3B). This overlap of processes is present but less pronounced between centra 2 and 3, and is absent between centra 3 and 4.

In addition, the first and second centra have a pair of horizontally oriented ribs that articulate with the associated centrum at dorsally located parapophyses (Fig. 3B; ribs not pictured). These ribs do not extend down to surround the viscera. On the first and second vertebral centra, the parapophyses are located at the base of the neural spine. On the third and fourth centra, the parapophyses are located more ventrally and articulate with ribs that extend down around the viscera (Fig. 3B). However, the parapophyses on vertebrae 3 and 4 are more dorsally located relative to the parapophyses on the abdominal rib-bearing vertebrae (Fig. 3B,D).

Vertebrae 5–10 have a typical abdominal vertebral morphology with reduced anterior and posterior dorsal processes and ventrally located parapophyses that articulate with ribs that extend ventrally around the viscera (Fig. 3C,D; ribs not pictured). In addition, a prominent lateral ridge of bone separates the dorsal and ventral portions of each vertebral centrum (Fig. 3D).

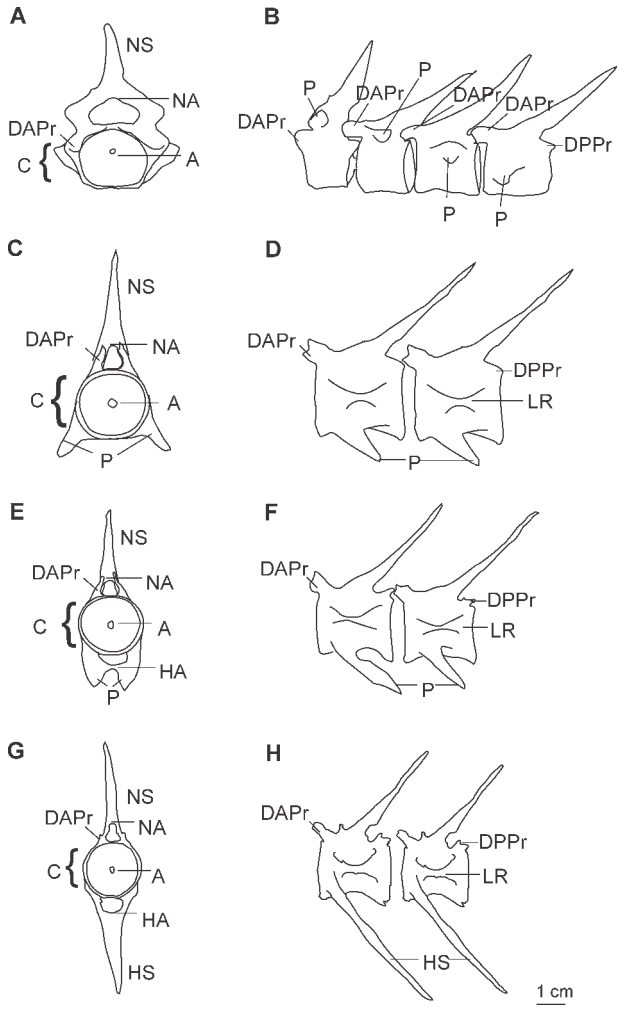

Fig. 3. Variation in gross morphology of vertebral centra along the length of the body axis in M. saxatilis. **A**: Anterior view of vertebra 1. **B**: Lateral view of vertebrae 1–4. **C**: Anterior view of vertebra 7. **D**: Lateral view of vertebrae 7 and 8. **E**: Anterior view of vertebra 11. **F**: Lateral view of vertebrae 11 and 12. **G**: Anterior view of vertebra 14. **H**: Lateral view of vertebrae 14 and 15. Abbreviations: A, amphicoel; C, centrum; DAPr, dorsal anterior process; DPPr, dorsal posterior process; HA, hemal arch; HS, hemal spine; LR, lateral ridge; NA, neural arch; NS, neural spine; P, parapophysis.

Vertebrae 11 and 12 have a transitional form with both hemal arches and ventrally located parapophyseal projections that articulate with ribs that extend ventrally around the viscera (Fig. 3E,F; ribs not pictured). Finally, vertebrae 13–23 have a typical caudal vertebral morphology with reduced dorsal processes relative to the first 4 vertebrae, an absence of ribs and parapophyseal articulations, and presence of hemal arches and spines (Fig. 3G,H). In addition, a prominent lateral ridge is now clear along the midline of each centrum in the transitional and caudal regions (Fig. 3F,H).

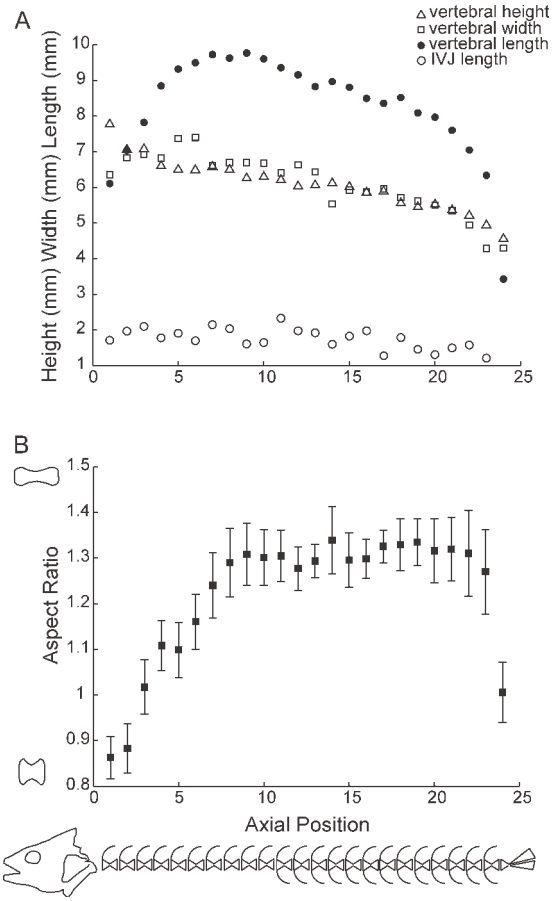

Fig. 4. Longitudinal variation in morphological measurements. **A**: Representative plot from Individual 01 of longitudinal variation in vertebral height, width, and length (triangles, squares, and closed circles, respectively). Each varied significantly along the length of the vertebral column ($P < 0.0001$, $P < 0.0001$, $P = 0.0002$, respectively; $n = 5$ fish). Variation of IVJ length (open circles) was not significant ($P = 0.4181$). **B**: Mean vertebral aspect ratio (length/width) (± 1 SD) for all five individuals along the length of the vertebral column. Note the increase in aspect ratio corresponding to an elongation of vertebral centra until approximately vertebra 8. Posterior to vertebra 8, the aspect ratio plateaus.

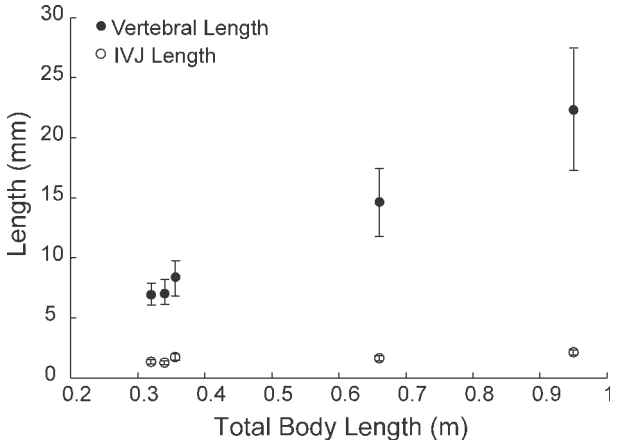

Fig. 5. Mean vertebral length and IVJ length relative to total body length. Each symbol represents one individual ($n = 5$ fish). The error bars show 1 SD and indicate the variation from cranial to caudal along the length of the vertebral column for each individual. Note that IVJ length varies less than expected across the threefold range of total body lengths investigated in these experiments. Vertebral length (closed circles) and IVJ length (open circles).

Gross Morphological Measurements

The length, height, and width of the vertebral centra all varied significantly with axial position ($F = 2.57$, d$f = 23.96$, $P = 0.0002$; $F = 10.44$, d$f = 23.96$, $P < 0.0001$; $F = 4.59$, d$f = 23.96$, $P < 0.0001$, respectively; $n = 5$ fish). Vertebral length increases initially from the first vertebra until approximately the eighth vertebra, beyond which the vertebral length declines through the caudal region. Vertebral height and width both show a steady decline from cranial to caudal (Fig. 4A).

This longitudinal variation in length and width produces variation in the aspect ratio (length/width) of the vertebral centra (Fig. 4B). There is a significant effect of axial position on the aspect ratio of the vertebral centra ($F = 5.39$, d$f = 23.96$, $P = 0.0013$). Qualitatively, the aspect ratio increases from the first vertebra until approximately vertebra 8. Aspect ratio plateaus through the caudal region and then there is a sudden drop in aspect ratio at the urostyle (Fig. 4B). It is important to note that the plateau region does not begin specifically at vertebra 8 in all individuals, but does occur between vertebrae 7–9 in the five individuals examined in this study.

In contrast to the length and width of the centra, the data for IVJ length (Fig. 4A) show no significant variation along the length of an individual ($F = 1.09$, d$f = 23.95$, $P = 0.4181$). For each individual, we see very little indication of variation along the length of the body axis, as portrayed by the small variance around each mean (Fig. 5). In addition, we see that despite the threefold variation in body length across the five individuals studied here, the IVJ length varies less than twofold, from 1.5 to 2.6 mm in length (Fig. 5 open circles, $r^2 = 0.49$, slope = 0.54). Vertebral length, by contrast, increases approximately in proportion with body length (Fig. 5 solid circles, $r^2 = 0.99$, slope = 1.1), and absolute variance within each fish increases in proportion to mean vertebral length (error bars, Fig. 5).

Histology

The amphicoels within the IVJs of the striped bass contain a mass of notochordal cells and two fluid-filled lacunae (Fig. 6A–D). Within the notochordal cells, there is variation in the presence and size of vacuoles. Elongated, unvacuolated notochordal cells surround the fluid filled lacunae, forming the notochordal epithelium. In addition, there

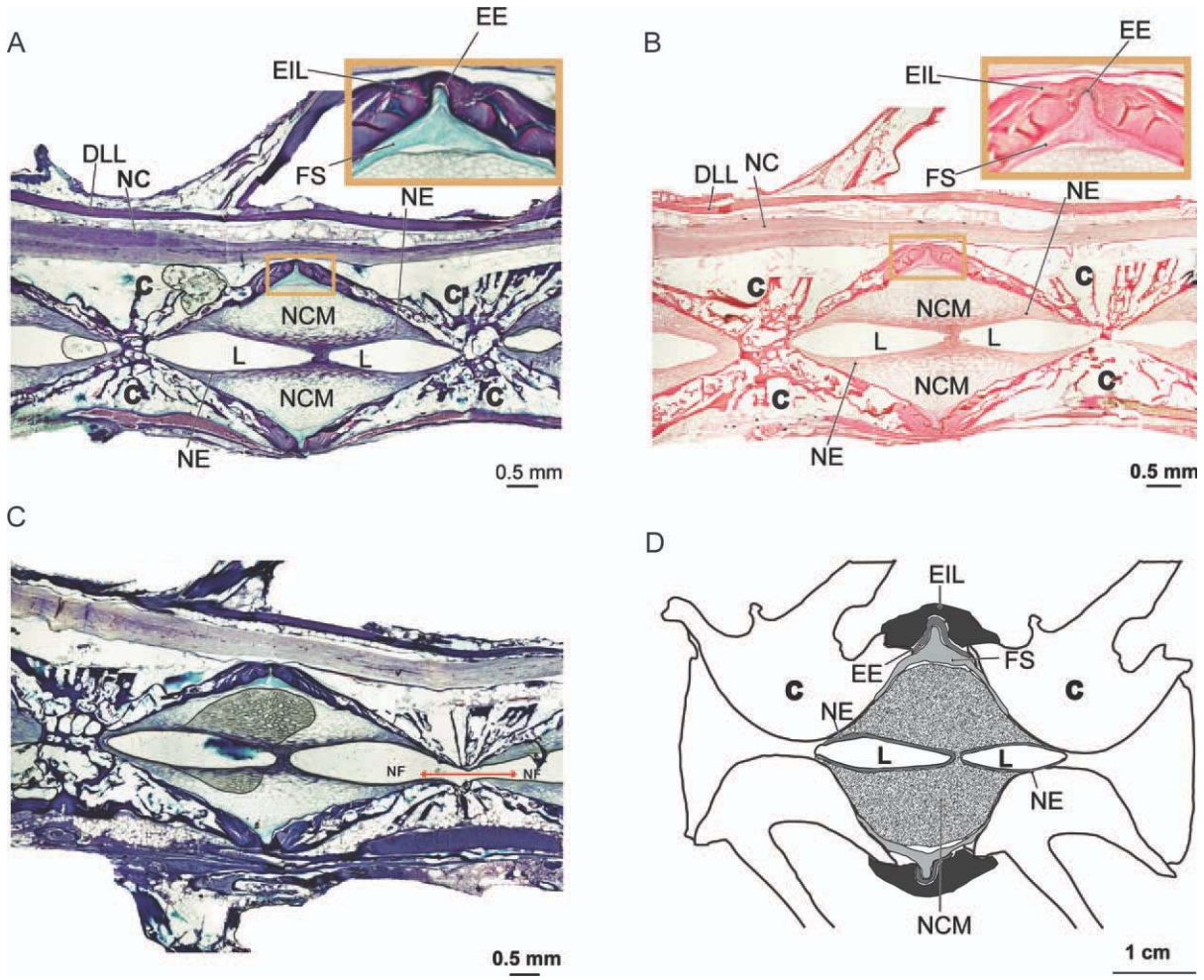

Fig. 6. Histology of the intervertebral joints of striped bass. **A**: Photomicrograph of one IVJ sectioned sagittally and stained with Masson's Trichrome stain. The inset shows a magnified view of the encapsulating complex tissues. **B**: An adjacent serial section stained with Verhoeff's elastin stain. Inset same as (A). **C**: Photomicrograph showing the patent notochordal foramen passing through the vertebral centrum on the right. **D**: Line drawing of the IVJ tissues. Abbreviations: C, centrum; DLL, dorsal longitudinal ligament; EE, elastica externa; EIL, external intervertebral ligament; FS, fibrous sheath; L, extracellular lacunae; NC, nerve cord; NCM, notochordal cell mass; NE, notochordal epithelium; NF, notochordal foramen.

appears to be a loss of vacuolization in the notochordal cells between the two fluid filled lacunae (Fig. 6A,B). There is no evidence of a notochordal strand extending the length of the vertebral column. However, a notochordal foramen is clearly visible in midsagittal sections from all three regions of the vertebral column examined in this study (Fig. 6C).

The encapsulating complex is composed of three tissue layers: the fibrous sheath, the elastica externa, and the external intervertebral ligament (Fig. 6A,B, insets,D). The fibrous sheath (Fig. 6A blue,D) is the deepest layer of the encapsulating tissues. It is thickened in the intervertebral region, but has narrow extensions lining the amphicoels. It appears to be acellular in the striped bass (Fig. 6A,B, insets). The elastica externa lies just superficial to the fibrous sheath, and is the only elastin-containing tissue in the joint (Fig. 6B black,D). The most superficial layer of the encapsulating tissues is the external intervertebral ligament (Fig. 6A inset purple,D). This tissue inserts on the outer rims of each amphicoelous cone. In addition, there is a dorsal longitudinal ligament situated dorsal to the nerve chord passing through the neural arches of the vertebrae (Fig. 6A,B). The histology of the IVJs is qualitatively similar in all three regions of the vertebral column of all three individuals examined.

Quantitatively, mean combined volume of the two lacunae per joint is 0.55 mm^3 in the cervical motion segment, 1.97 mm^3 in the abdominal motion segment, and 1.15 mm^3 in the caudal motion segment (Table 2). However, these differences are not statistically significant ($F = 2.38$, $df = 2.6$, $P = 0.174$). We see a pattern of decrease in tissue volume from cranial to caudal in the remaining tissues: the notochordal cell mass, the fibrous sheath, the elastica externa, the external intervertebral ligament, and the dorsal longitudinal ligament. The variation in

TABLE 2. Mean IVJ tissue measurements (±1 SD; n = 3 fish)

	Cervical	Abdominal	Caudal	*P*-Value
Lacunae vol. (mm^3)	0.55 ± 0.22	1.97 ± 1.31	1.15 ± 0.02	$P = 0.174$
Lacunae % of IVJ volume	3.9%	12.8%	11.3%	—
NCM volume (mm^3)	13.27 ± 2.00	12.91 ± 2.10	8.90 ± 1.24	$P = 0.046$*
NCM % of IVJ volume	96.1%	87.2%	88.7%	—
Fibrous sheath vol. (mm^3)	1.67 ± 0.45	0.85 ± 0.39	0.63 ± 0.35	$P = 0.042$*
Fibrous sheath CSA (mm^2)	2.01 ± 0.59	1.02 ± 0.50	0.77 ± 0.48	$P = 0.062$
Elastica externa vol. (mm^3)	0.24 ± 0.09	0.14 ± 0.02	0.13 ± 0.04	$P = 0.138$
Elastica externa CSA (mm^2)	0.29 ± 0.12	0.17 ± 0.03	0.16 ± 0.06	$P = 0.165$
EIL vol. (mm^3)	2.21 ± 0.69	1.71 ± 0.54	1.51 ± 0.49	$P = 0.400$
EIL CSA (mm^2)	2.64 ± 0.79	2.05 ± 0.72	1.82 ± 0.74	$P = 0.438$
DLL vol. (mm^3)	0.12 ± 0.01	0.10 ± 0.09	0.05 ± 0.02	$P = 0.284$
DLL CSA (mm^2)	0.15 ± 0.02	0.12 ± 0.10	0.06 ± 0.03	$P = 0.265$

*Significant at 0.05 level, df = 2.6 for all tissues; see text for F-values. Statistical analysis was only performed on the raw values and not on the percentages.

the notochordal cell and fibrous sheath volumes are statistically significant ($F = 5.35$, d$f = 2.6$, $P = 0.046$ and $F = 5.61$, d$f = 2.6$, $P = 0.042$, respectively). However, when the cross-sectional area of the fibrous sheath is calculated the trend is marginally insignificant ($F = 4.59$, d$f = 2.6$, $P = 0.062$). The remaining variation in IVJ tissues is not statistically significant (Table 2).

Polarized Light Imaging

Qualitatively, there is variation in the number of fiber populations that compose the vertical septum along the length of the vertebral column (Fig. 7). In the cervical region, we see four different fiber populations with distinct trajectories: an anterior–posterior population (purple), a dorso–ventral oblique population (green), a ventro–dorsal oblique population (gray), and a dorso–ventral population (yellow, Fig. 7A,B). In addition, we see fibers inserting not only on the neural spines but also on the pterygiophores that extend down between the spines (Fig. 7A). A similar organization of four fiber populations is found in the abdominal region as well (Fig. 7C,D). In contrast, there is only one population of fibers in the vertical septum of the caudal region of the fish. This fiber population is oriented dorso–ventrally (yellow) and is found between both the neural and hemal spines (Fig. 7E,F).

A nested ANOVA and post hoc Tukey analysis ($n = 3$ fish) reveals significant differences in the angles of insertion of the dorso–ventral oblique (green) fiber population between the rostral regions. The angle of insertion of these fibers varies from $126^\circ \pm 7.4^\circ$ in the cervical region to $105^\circ \pm 6.3^\circ$ in the abdominal region ($F = 15.05$, d$f = 1.4$, $P = 0.018$). The angles of insertion of the remaining three fiber populations are similar along the length of the vertebral column.

DISCUSSION

Our investigations of vertebral and IVJ morphology reveal significant regional variation in gross vertebral morphology, IVJ histology, and collagen fiber populations in the vertical septum. These results support the designation of a cervical region of the striped bass vertebral column, distinct from the rest of the abdominal vertebrae. Vertebral centrum length is the greatest in the abdominal region and decreases anteriorly (cervical region) and posteriorly (caudal region). Notochordal cell volume is greatest in the cervical region and decreases in the abdominal and caudal regions. Vertebral width and height decrease from cranial to caudal, but IVJ length remains constant along the length of the fish. Finally, the vertical septum decreases in complexity in the caudal region. This variation in both bony and soft tissue morphology suggests that the caudal IVJs may have a greater range of motion and decreased stiffness relative to the more anterior joints.

Regionalization

The results of this study provide qualitative and quantitative support for the recognition of a distinct cervical region in *M. saxatilis*. There is gross morphological variation between vertebral centra 1–4 compared with vertebral centra 5–10. The degree of articulation of the dorsal anterior processes and dorsal posterior processes of the first 4 vertebrae is substantially greater. In addition, the more dorsal location of parapophyses on the first 4 vertebrae contrasts with the ventrally located parapophyses of the remaining abdominal centra (Fig. 3B,D). Thus, based on the bony projections and rib morphology of these first 4 vertebrae, we believe that a separate cervical region should be recognized.

Quantitatively, the results of the present study show significant differences in the aspect ratio, notochordal cell volumes, and fibrous sheath volumes between the cervical joints and the abdominal joints. In addition, despite having the same number of fiber populations in the vertical septum, there are significant differences in the insertion

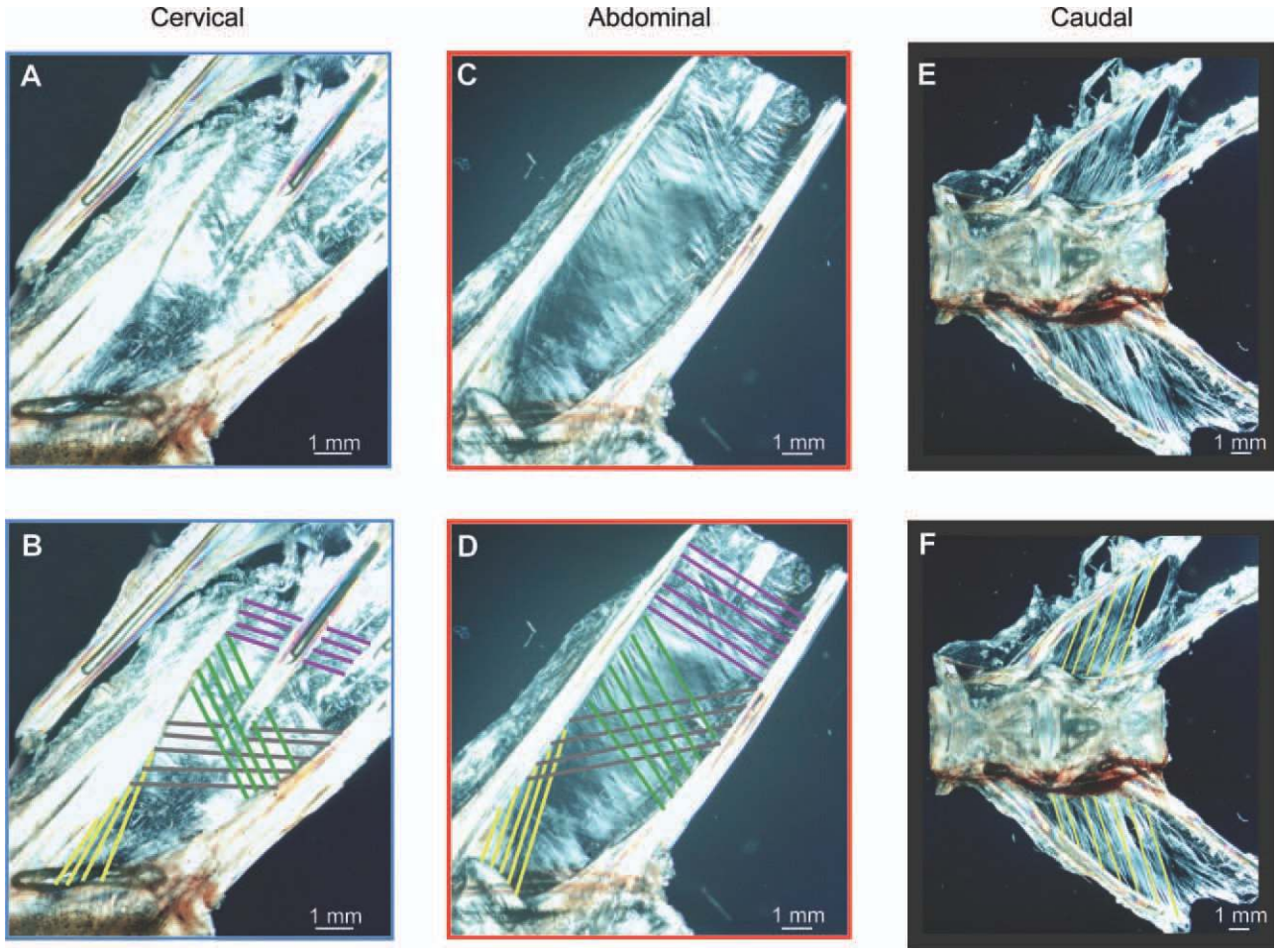

Fig. 7. Polarized light photomicrographs of the vertical septum. **A**: Cervical region. **B**: Traces the four fiber populations in the cervical region. **C**: Abdominal region. **D**: Traces the four fiber populations in the abdominal region. **E**: Caudal region. **F**: Traces the one fiber population in the caudal region. The following four fiber populations were identified along the length of the vertebral column: anterior–posterior (purple), dorso–ventral oblique (green), ventro–dorsal oblique (gray), and dorso–ventral (yellow). Note that only the dorso–ventral population is found in the caudal region of the fish.

angles of the dorso–ventral oblique population between the cervical and abdominal joints.

Gross morphology is evidence of a transitional region for vertebrae 11–12 (Fig. 3E,F). These vertebrae have hemal arches while still retaining ribs (Bird and Mabee, 2003). However, because the histological preparations and vertical septum imaging were not done for these vertebrae, we do not have any more support for including these transitional vertebrae as a separate region.

Accurate vertebral column regionalization requires not only morphological investigation, but also mechanical and kinematic investigation to link variation in form to variation in function. Although these morphological data are indicative of a distinct cervical region, mechanical testing and kinematic analyses of these joints are required to discern whether the variation in anatomy described in this study has any impact on the function of the vertebral column in the cervical region of striped bass.

Notochordal Foramen

Our finding of a notochordal foramen in the striped bass is worthy of mention. This structure has been described previously, but it has been suggested that it exists only in basal fish taxa that have a notochordal strand (Symmons, 1979). However, here we see an example of a perciform fish with a patent notochordal foramen along the length of the vertebral column in the absence of a notochordal strand. In addition, we see that the fluid filled lacunae clearly pass through this notochordal foramen creating a continuous, dumbbell-shaped lacuna that spans the two joints that the vertebral centrum is associated with (Fig. 6C). Consequently, it is possible that fluid may be able to pass through the notochordal foramen. However, the mean diameter of the foramen is ~0.16 mm, and therefore, would require a large pressure differential to facilitate this fluid movement.

Functional Implications

The variation in vertebral shape along the length of the axial skeleton may have functional implications relevant to the lateral bending of the body. The centra become narrow and more elongate from the cervical region to the mid-abdominal region (approximately vertebra 8) and then decrease in length while continuing to decrease in width through the caudal region. This is most evident when considering the aspect ratio (Fig. 4B). Initially, length increases as width decreases. Therefore, we see an increase in the aspect ratio. However, as length begins to decrease at a similar rate as width, the aspect ratio plateaus. At the same time, the IVJ length remains constant along the length of the vertebral column. Given the constant length of the IVJs, this suggests a greater range of motion during lateral bending in the caudal region. As the width of the vertebrae decreases, if one were to allow the vertebrae to bend laterally until the rims of the adjacent bones came into contact with one another, the narrower vertebrae in the caudal region of the fish would subtend a larger angle of bending (Fig. 8A,B). If we assume that each pair of vertebrae rotates about the center of the joint, we can use the radius of each centrum and the IVJ length to estimate the maximum range of motion between each pair of vertebrae along the vertebral column using the law of cosines (Fig. 8A,B):

$$\alpha = \mathrm{acos}((rC1^2 + rC2^2 - \mathrm{IVJ\,length}^2)/(2{\times}rC1rC2))$$

where $rC1$ is the radius of the anterior centrum and $rC2$ is the radius of the posterior centrum. When the angle between each pair of vertebrae along the length of the vertebral column is calculated, we find that the hypothesis that the narrower caudal IVJs will attain a larger range of motion is supported (Fig. 8C). It is important to note that this hypothesis is based only on vertebral morphology and IVJ length, and does not include the function of the IVJ tissues in resisting bending. Thus, the angles calculated here are likely higher than those expected in vivo; however, we expect the trend of greater caudal range of motion to hold true. Further, in vivo kinematic analysis is necessary to test this idea.

In addition, the decrease in the notochordal cell mass within the joint capsule suggests a decrease in stiffness in the caudal IVJs (Table 2). The vacuole within each notochordal cell is thought to contain an incompressible aqueous solution capable of resisting compressive forces, and is surrounded by a dense network of intermediate filaments thought to be capable of resisting tensile forces. The network of intermediate filaments within each vacuolated cell is connected to the networks of the adjacent cells via the desmosomes. In this way, the mass of vacuolated cells is hypothesized to act as a hydrostat, resisting the compressive and tensile forces associated with lateral bending during swimming and thereby increasing the stiffness of the IVJ (Schmitz, 1995). Given this hypothesis, the decrease in the volume of notochordal cells in the caudal region shown in this study should result in decreased stiffness of those joints.

Similarly, the incompressible fluid within the extracellular lacunae is also thought to resist

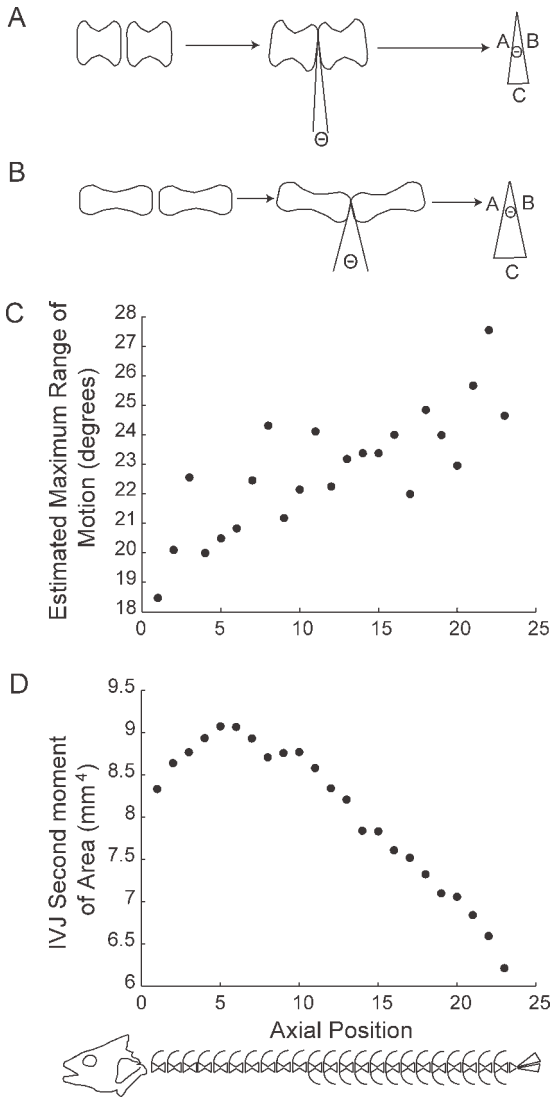

Fig. 8. Estimated range of motion and stiffness based on vertebral centrum diameter, IVJ length, and second moment of area (Ic). Schematic showing a pair of large diameter centra (**A**) and small diameter centra (**B**) in resting position and in a bent position. Using half the width of the anterior vertebra, length A, and half the width of the posterior vertebra, length B, and the IVJ length we create triangles of known side lengths to calculate a rough estimate of range of motion based on the law of cosines. **C**: Estimated range of motion for each joint based on the vertebral radius and IVJ length measurements of the five individuals from the present study. **D**: Second moment of area (I_c) calculations indicate that the caudal joints will have the lowest angular stiffness while the abdominal joints will have the greatest.

compressive forces associated with locomotion. The squamous, nonvacuolated cells lining the lacunae and separating the two lacunae in the intervertebral septum contain dense intermediate filaments. The adjacent cells adhere to one another via desmosomal connections that are thought to resist shearing forces (Schmitz, 1995). Thus, the extracellular lacunae are thought to increase joint stiffness hydrostatically as well (Schmitz, 1995). The results of this study do not yield a clear conclusion about longitudinal variation in the volumes of the extracellular lacunae. Mean lacuna size was largest in the abdominal region and smaller in the cervical region and the caudal region (Table 2). Although this variation was not significant, it again points towards decreased stiffness in the caudal joints, and possibly the cervical joints, compared with the abdominal joints.

The volume of the fibrous sheath decreases significantly along the length of the vertebral column (Table 2). This decreasing trend holds when the cross-sectional area of the tissue is calculated, however, the result is no longer significant. This discrepancy is likely related to the small sample size included in the analysis, thus the results should be viewed with caution. The fibrous sheath is thought to be made up of helically wound, type II collagen, similar to the fibrous sheath of cyclostomes and tetrapods (Linsenmayer et al., 1973; Kimura and Kamimura, 1982; Eikenberry et al., 1984; Schmitz, 1998). Additionally, the fibrous sheath of the striped bass lines the bony cone of the amphicoel and thickens in the intervertebral region (Fig. 6A,B). In this manner, the fibrous sheath connects the two adjacent vertebrae, and thus, likely plays a role in resisting loading during bending. The decrease in the volume of this fibrous sheath from cranial to caudal suggests a potential decrease in IVJ stiffness along the length of the fish.

These differences in soft tissue anatomy all suggest a decrease in stiffness along the length of the vertebral column. These structural tissues should influence the second moment of area, a structural predictor of flexural stiffness, of each IVJ. Specifically, the encapsulating tissues should have the greatest impact on the second moment of area because they are located furthest from the neutral axis of bending. Thus, we expect a decline in the second moment of area from cranial to caudal associated with the decline of the fibrous sheath and possibly the notochordal cell mass.

If we model the encapsulating tissues of each IVJ as circular in cross section (see Porter et al., 2009), we can calculate the second moment of area with the following equation:

$$I_c = \pi r^4/4$$

where r is the estimated radius of each IVJ taken as the average of the height and transverse width of the associated anterior centrum. The mean I_c across the five individuals results in an initial increase in stiffness from the cervical to the abdominal region, and then a decline in stiffness through the caudal region (Fig. 8D). This initial increase indicates that the flexural stiffness of the cervical joints may actually be less than the abdominal joints. This again supports the inclusion of a distinct cervical region, although it is in contrast to our predictions of greater stiffness in the most rostral joints. All the rostral joints, however, appear to have greater flexural stiffness than the caudal region, again indicating decreased stiffness caudally.

It is important to note that engineering theory assumes a homogenous material when calculating the second moment of area. The IVJs violate this assumption and are not exactly circular in cross section. However, this simplified model does indicate that the variation in anatomy revealed in this study should result in decreased structural stiffness in the caudal region of the vertebral column. Further, mechanical testing is necessary to support this hypothesis.

Finally, this study has shown a substantial difference in the number of fiber populations found in the vertical septum along the length of an individual striped bass (Fig. 7). In the cervical and abdominal regions of the fish, we identify four fiber populations with distinct trajectories. However, in the caudal region of the fish, only one fiber population is present (Fig. 7C,F). If the vertical septum plays a role in resisting bending during swimming, this variation in fiber population again points toward lower stiffness in the caudal region of the fish, relative to the cervical and abominal regions.

These morphological results consistently predict a decrease in stiffness and an increase in the range of motion in the caudal region of the striped bass. However, previous studies in the blue marlin show increased joint stiffness caudally (Hebrank et al., 1990; Long, 1992). In addition, investigation of the mechanics of Norfolk spot found uniform stiffness along the length of the spine (Hebrank, 1982). These previous mechanical results do not agree with our morphological findings. Thus, further mechanical analysis is necessary to determine whether the morphological regionalization described here corresponds to mechanical regionalization of the striped bass vertebral column.

ACKNOWLEDGMENTS

The authors thank Susquehanna Aquaculture, Inc. for providing the live animals for this study. They also thank Eric LoPresti and Nicholas Gidmark for help with fish housing and husbandry. A special thanks to Steve Gatesy, Thomas Roberts, Sharon Swartz, John Long, Manny Azizi, Erika

Giblin, and the Morphology Group at Brown for helpful discussion and suggestions.

LITERATURE CITED

Bird NC, Mabee PM. 2003. Developmental morphology of the axial skeleton of the Zebrafish, *Danio rerio* (Ostariophysi: Cyprinidae). Dev Dyn 228:337–357.

Bond CE. 1996. Biology of Fishes, 2nd ed. Philadelphia: Saunders College Publishing.

Burke AC, Nelson CE, Morgan BA, Tabin C. 1995. Hox genes and the evolution of vertebrate axial morphology. Development 121:333–346.

Eikenberry EF, Childs B, Sheren SB, Parry DAD, Craig AS, Brodsky B. 1984. Crystalline fibril structure of type II collagen in lamprey notochord sheath. J Mol Biol 176:261–277.

Gadow H, Abbott EC. 1895. On the evolution of the vertebral column of fishes. Philos Trans R Soc London B 186:163–221.

Grande L, Bemis WE. 1998. A comprehensive phylogenetic study of amiid fishes (Amiidae) based on comparative skeletal anatomy. An empirical search for interconnected patterns of natural history. J Vertebr Paleontol 18:1–690.

Grotmol S, Kryvi H, Keynes R, Krossoy C, Nordvik K, Totland GK. 2006. Stepwise enforcement of the notochord and its intersection with the myoseptum: An evolutionary path leading to development of the vertebra? J Anat 209:339–357.

Gurr E. 1962. Staining Animal Tissues: Practical and Theoretical. London: L. Hill.

Hamilton JL, Dillaman RM, McLellan WA, Pabst DA. 2004. Structural fiber reinforcement of keel blubber in harbor porpoise (*Phocoena phocoena*). J Morph (2004) 261:105–117.

Harper CJ, McLellan WA, Rommel SA, Gay DM, Dillaman RM, Pabst DA. 2008. Morphology of the melon and its tendinous connections to the facial muscles in bottlenose dolphins (*Tursiops truncatus*). J Morph 269:820–839.

Hebrank MR. 1982. Mechanical properties of fish backbones in lateral bending and tension. J Biomech 15:85–89.

Hebrank JH, Hebrank MR, Long JH, Block BA, Wainwright SA. 1990. Backbone mechanics of the blue marlin *Makaira nigricans* (Pisces, Istiophoridae). J Exp Biol 148:449–459.

Heilman G. 1927. The Origin of Birds. New York: D. Appelton and Company.

Helfman GS, Collette BB, Facey DE. 1997. The Diversity of Fishes. Malden: Blackwell Science.

Humason GL. 1979. Animal Tissue Techniques, 4th ed. San Francisco: WH Freeman and Company.

Junqueira L, Carneiro,J. 2005. Basic Histology, 11th ed. Columbus: McGraw-Hill Medical.

Kacem A, Meunier FJ, Bagliniere JL. 1998. A quantitative study of morphological and histological changes in the skeleton of *Salmo salar* during its anadromous migration. J Fish Biol 53:1096–1109.

Kardong KV. 1998. Vertebrates: Comparative Anatomy, Function, Evolution. Boston: WCB/McGraw-Hill.

Kimura S, Kimimura,T. 1982. Characterization of lamprey notochord collagen with special reference to its skin collagen. Comp Biochem Physiol 73B:335–339.

Kulig K, Powers CM, Landel RF, Chen H, Fredericson M, Guillet M, Butts K. 2007. Segmental lumbar mobility in individuals with low back pain: In vivo assessment during manual and self-imposed motion using dynamic MRI. BMC Musculoskelet Disord 8:8–18.

Liem KF, Bemis WE, Walker WF, Grande L. 2001. Functional Anatomy of the Vertebrates, 3rd ed. Belmont: Brooks Cole.

Linsenmayer TF, Trelstad RL, Gross J. 1973. The collagen of chick embryonic notochord. Biochem Biophys Res Commun 53:39–45.

Long JH. 1992. Stiffness and damping forces in the intervertebral joints of blue marlin (*Makaira nigricans*). J Exp Biol 162:131–155.

McDonald CP, Bachison CC, Chang V, Bartol SW, Bey MJ. 2010. Three-dimensional dynamic in vivo motion of the cervical spine: Assessment of measurement accuracy and preliminary findings. Spine J 10:497–504.

Morin-Kensicki EM, Melancon E, Eisen JS. 2002. Segmental relationship between somites and vertebral column in zebrafish. Development 129:3851–3860.

Nordvik K, Kryvi H, Totland GK, Grotmol S. 2005. The salmon vertebral body develops through mineralization of two preformed tissues that are encompassed by two layers of bone. J Anat 206:103–114.

Panjabi MM, Brand RA, White AA. 1976. Mechanical properties of the human thoracic spine as shown by three-dimensional load-displacement curves. J Bone Joint Surg Am 58:642–652.

Panjabi MM, Oxland TR, Yamamoto I, Crisco JJ. 1994. Mechanical behavior of the human lumbar and lumbosacral spine as shown by three-dimensional load-displacement curves. J Bone Joint Surg Am 76:413–424.

Panjabi MM, Crisco JJ, Vasavada A, Oda T, Cholewicki J, Nibu K, Shin E. 2001. Mechanical properties of the human cervical spine as shown by three-dimensional load-displacement curves. Spine 26:2692–2700.

Porter ME, Roque CM, Long JH. 2009. Turning maneuvers in sharks: Predicting body curvature from axial morphology. J Morph 270:954–965.

Presnell J, Schreibman M. 1997. Humanson's Animal Tissue Techniques. Baltimore: Johns Hopkins University Press.

Rockwell H, Evans FG, Homer,CP. 1938. The comparative morphology of the vertebrate spinal column. Its form as related to function. J Morph 63:87–117.

Romer AS. 1956. Osteology of Reptiles. Chicago: University of Chicago Press.

Schmitz RJ. 1995. Ultrastructure and function of cellular components of the intercentral joint in the percoid vertebral column. J Morph 226:1–24.

Schmitz RJ. 1998. Comparative ultrastructure of the cellular components of the unconstricted notochord in the sturgeon and the lungfish. J Morphol 236:75–104.

Symmons S. 1979. Notochordal and elastic components of the axial skeleton of fishes and their functions in locomotion. J Zool 189:157–206.

Videler JJ. 1993. Fish Swimming. London: Chapman and Hall.

Wake MH. 1980. Morphometrics of the skeleton of *Dermophis mexicanus* (Amphibia: Gymnophiona). I. The vertebrae, with comparisons to other species. J Morph 165:117–130.

Wake DB, Lawson RL. 1973. Developmental and adult morphology of the vertebral column in the plethodontid salamander *Eurycea bislineata*, with comments on vertebral evolution in the amphibia. J Morph 139:251–300.

Ward AB, Brainerd EL. 2007. Evolution of axial patterning in elongate fishes. Biol J Linn Soc 90:97–116.

White A, Panjabi MM. 1978. Clinical Biomechanics of the Spine, 2nd ed. Philadelphia: Lippincott Williams and Wilkins.

Witten PE, Hall BK. 2003. Seasonal changes in the lower jaw skeleton in male Atlantic salmon (*Salmo salar* L): Remodeling and regression of the kype after spawning. J Anat 203:435–450.